

PHOTOPHORETIC STRUCTURING OF CIRCUMSTELLAR DUST DISKS

TAKU TAKEUCHI¹ AND OLIVER KRAUSS²

Received 2007 January 16; accepted 2007 December 2

ABSTRACT

We study dust accumulation by photophoresis in optically thin gas disks. Using formulae for the photophoretic force that are applicable for the free molecular regime and for the slip-flow regime, we calculate dust accumulation distances as a function of particle size. It is found that photophoresis pushes particles (smaller than 10 cm) outward. For a Sun-like star, these particles are transported to 0.1–100 AU, depending on their size, and form an inner disk. Radiation pressure pushes small particles (≤ 1 mm) out further to form an extended outer disk. Consequently, an inner hole opens inside ~ 0.1 AU. The radius of the inner hole is determined by the condition that the mean free path of the gas molecules equal the maximum size of the particles that photophoresis effectively works on (100 μm –10 cm, depending on the dust properties). The dust disk structure formed by photophoresis can be distinguished from the structure of model gas-free dust disks, because the particle sizes in the outer disk are larger, and the inner hole radius depends on the gas density.

Subject headings: circumstellar matter — planetary systems: formation — solar system: formation

1. INTRODUCTION

Protoplanetary disks are composed of gas and dust. In the initial stages of their evolution, protoplanetary disks contain as much as 10^{-3} to $10^{-1} M_{\odot}$ of gas (Greaves 2004), and small dust particles are mixed with the gas, making the disks optically thick at optical wavelengths. As the dust particles grow, the number of small particles is reduced, and at a certain stage the disk becomes optically thin (Tanaka et al. 2005; Dullemond & Dominik 2005). The amount of gas also decreases, as the gas dissipates (see, e.g., Hartmann et al. 1998; Clarke et al. 2001; Takeuchi et al. 2005; Alexander et al. 2006a, 2006b). In the late stages of the disk evolution, they become gas-free dust disks, which are observed as Vega-type disks. During the transition from a protoplanetary to a Vega-type disk, there may be a stage in which the disk is optically thin but the gas component still remains. An example is HD 141569A, which is a 5 Myr old Herbig Be star (Weinberger et al. 2000) and has an optically thin dust disk (Augereau et al. 1999; Weinberger et al. 1999; Fisher et al. 2000; Mouillet et al. 2001; Marsh et al. 2002; Clampin et al. 2003). The gas component of this system has been observed (Zuckerman 1995; Dent et al. 2005; Goto et al. 2006) and is estimated to amount to $\lesssim 60 M_{\oplus}$ (Ardila et al. 2005).

The dynamics of dust particles in optically thin gas disks is of interest in order to investigate the structure of transitional disks. Krauss & Wurm (2005) considered the motion of dust particles in a gas disk that is optically thin at optical wavelengths. A dust particle receives stellar radiation directly, and the radiation pressure pushes it outward. In addition to radiation pressure, the interaction between the particle and the surrounding gas molecules induces photophoresis, which also pushes it outward (see also Wurm & Krauss 2006; Krauss et al. 2007). When these outward accelerations act with the gas drag on the particle, the particle drifts outward (Takeuchi & Artymowicz 2001). In the outer part of the disk ($\gtrsim 10$ AU), where the mean free path of the gas molecules is larger than the particle size ($\lesssim 1$ m), the photophoretic force is proportional to the gas density. When a particle moves

outward to a point where the gas density is no longer high enough to induce a strong photophoretic force, the particle's outward motion stops. Consequently, the dust particles pile up at a certain distance from the star that is determined by the density profile of the gas disk. In a disk with mass $\sim 0.01 M_{\odot}$, particles of 100 μm to 10 cm pile up at several tens of AU. This spontaneous ring formation is a characteristic feature that is caused by photophoresis in a gaseous dust disk.

Krauss et al. (2007) have demonstrated that photophoretic dust motion may be the key process in the transition from optically thick protoplanetary disks to optically thin circumstellar disks with ringlike dust distributions, via the stage of a transitional disk with an inner hole and a more or less sharp transition to the outer disk that is continuously pushed outward. This outward dust migration can also explain the presence of material formed close to the Sun such as chondrules and Ca-Al-rich inclusions (CAIs) in main-belt asteroids (Wurm & Krauss 2006) or high-temperature crystalline silicates in comets from the Kuiper Belt (Petit et al. 2006; Brownlee et al. 2006; Mousis et al. 2007).

In this paper, we seek to investigate other characteristic structures formed by photophoresis, especially in the inner part of the disk, but at a stage when most of the dust has already built up into larger bodies. Krauss & Wurm (2005) focused on the dust dynamics in the outer part of the disk ($\gtrsim 10$ AU) and used a formula for the photophoretic force that is relevant for low gas densities. In order to investigate the structure of the whole disk, we use a photophoresis formula that can be applied to the whole range of gas densities. Details of the formula adopted here are described in § 2. Using this formula, we find that photophoresis does not induce dust pileup in the innermost region of the disk (≤ 0.1 AU), leading to the formation of an inner hole (see § 3). In the inner part of the gas disk, the gas density may be so high that the disk itself is no longer optically thin to the stellar radiation, and thus radiation effects such as radiation pressure and photophoresis will not work on the dust at all. In order to investigate whether photophoresis still works at the inner disk, in § 4 we calculate the optical depth of the disk due to Rayleigh scattering by the hydrogen molecules. In § 5.1, the thermal relaxation time of the dust particles is estimated and compared with the rotation periods induced by gas turbulence and by photophoresis. In § 5.2, we discuss the characteristic features that photophoresis forms in dust

¹ Department of Earth and Planetary Sciences, Kobe University, Kobe 657-8501, Japan; taku@kobe-u.ac.jp.

² Institut für Planetologie, Westfälische Wilhelms-Universität Münster, D-48149 Münster, Germany; okrauss@uni-muenster.de.

disks and what observable differences there are from the structures produced by gas-free dust disks. In Appendix A, a simple calculation deriving the photophoretic force is described.

2. RADIAL DRIFT OF DUST PARTICLES

2.1. Forces Acting on Dust Particles

We consider the motion of a dust particle that resides in a gas disk around a star. The disk is assumed to be optically thin in the radial direction. This means that the dust particle directly receives the radiation from the central star. The stellar radiation that is absorbed or scattered by the particle pushes it outward. This outward force, which is called radiation pressure (Burns et al. 1979), is given by

$$F_{\text{rad}} = \pi a^2 Q_{\text{rad}} I / c, \quad (1)$$

where we assume that the particle is spherical and its radius is a , Q_{rad} is the efficiency factor of the radiation pressure and assumed to be unity in this paper, and c is the speed of light. We assume that the particle is on the midplane of the gas disk and its distance from the central star is r . The stellar radiation flux at the particle's position is

$$I = L / (4\pi r^2), \quad (2)$$

where L is the luminosity of the central star. Poynting-Robertson (P-R) drag can be neglected compared with gas drag. Even in a gas disk whose mass is as small as several Earth masses, gas drag is much stronger than P-R drag, as discussed below (§ 3.4; see also Takeuchi & Artymowicz 2001).

If the particle's hemisphere facing the central star becomes hotter than the opposite hemisphere, the particle receives the photophoretic force in addition to radiation pressure. Because, in general, the particle rotates with a certain speed, a considerable temperature gradient appears only if the thermal relaxation time of the particle is much smaller than its rotation period (see discussion in § 5.1) or if the rotation axis is aligned in the direction of the light source (Krauss et al. 2007). In this paper, we assume that the effect of the particle's rotation can be neglected. In this case, the photophoretic force is radially directed and its value can be analytically calculated. In Appendix A, we describe an estimate of the photophoretic force derived with a simple model of cylindrical dust particles, but we use the rigorous formulae that have been derived in the literature in the following discussion.

We consider a spherical dust particle of radius a . The mean temperature T_d of the particle is in general different from the surrounding gas temperature T_g . In this paper, we simply assume that $T_d = T_g$. The temperature gradient inside the particle is assumed to be small, and so the photophoretic force is calculated by solving a linearized perturbation equation for the temperature. In Appendix A, we discuss cases in which the above assumptions are not valid.

If the particle radius a is much smaller than the mean free path of the surrounding gas molecules l , that is, if the Knudsen number $\text{Kn} \equiv l/a \gg 1$, then the photophoretic force is calculated with the free molecular approximation (Hidy & Brock 1967; Mackowski 1989; Beresnev et al. 1993) and is given by

$$F_{\text{ph},f} = \frac{\pi \alpha J_1 P I a^2}{3(k_d T_d / a + 4\epsilon \sigma_{\text{SB}} T_d^4 + \alpha P v_T / 2)}, \quad (3)$$

where P is the gas pressure, k_d is the thermal conductivity inside the particle, ϵ is the particle's thermal emissivity and assumed to

be unity, σ_{SB} is the Stefan-Boltzmann constant, and v_T is the mean thermal velocity of the gas molecules. The asymmetry parameter J_1 represents how effectively the incident starlight induces a temperature gradient inside the particle. If the incident light is perfectly absorbed at the particle's surface, the asymmetry parameter J_1 has the maximum value 0.5, becoming smaller as the temperature gradient becomes smaller. We assume that the gas molecules leaving the particle after collision have a Maxwellian velocity distribution corresponding to the local surface temperature of the particle (i.e., the accommodation factor $\alpha = 1$). In many cases, the denominator of equation (3) is dominated by the first or second term; that is, the temperature gradient in the particle is determined by the internal thermal conduction or by the radiative cooling, rather than by the thermal conduction to the gas. In this case, the photophoretic force is approximated as

$$F_{\text{ph},f} \approx \frac{\pi \alpha J_1 k_B I a^2}{3\sqrt{2} \sigma_{\text{mol}} k_d (1 + 4\epsilon \sigma_{\text{SB}} T_d^3 a / k_d)} \text{Kn}^{-1}, \quad (4)$$

where we have used $P = n_g k_B T_g$ and where $l = 1/(\sqrt{2} n_g \sigma_{\text{mol}})$ and n_g is the number density of the gas molecules, k_B is the Boltzmann constant, and σ_{mol} is the collisional cross section of the gas molecules. In the free molecular regime, the photophoretic force is inversely proportional to the gas mean free path and thus proportional to the gas density.

If the particle size, a , is much larger than the mean free path of the gas molecules, l , that is, the Knudsen number $\text{Kn} \ll 1$, then the photophoretic force is calculated with the slip-flow approximation (Mackowski 1989). Mackowski (1989) calculated the photophoretic force assuming that the thermal radiation from the particle surface can be neglected. When the thermal radiation is taken into account, his formula is modified to

$$F_{\text{ph},s} = \frac{4\sqrt{2} C_s J_1 k_B I a^2}{k_d \sigma_{\text{mol}} d} \text{Kn} \quad (5)$$

(see Appendix B for the derivation), where

$$d = (1 + 3C_m \text{Kn}) \left[\left(\frac{4\epsilon \sigma_{\text{SB}} T_d^3 a}{k_d} + 1 \right) (1 + 2C_t \text{Kn}) + 2 \frac{k_g}{k_d} \right] \quad (6)$$

and C_s , C_m , and C_t are the coefficients for the jump conditions at the surface and are of order unity. We adopt the values $C_s = 1.17$, $C_m = 1.14$, and $C_t = 2.18$ (Mackowski 1989). The thermal conductivity of the gas is

$$k_g = (15/8) l v_T n_g k_B, \quad (7)$$

where we set the Prandtl number to $\frac{2}{3}$. When d is approximately unity—that is, $\text{Kn} \ll 1$, $4\epsilon \sigma_{\text{SB}} T_d^3 a / k_d \ll 1$, and $k_g / k_d \ll 1$ —the photophoretic force is proportional to the gas mean free path.

To connect the above two regimes, we introduce the following formula:

$$F_{\text{ph}} = \frac{\text{Kn}^2 F_{\text{ph},f} + F_{\text{ph},s}}{1 + \text{Kn}^2}. \quad (8)$$

In the limit $\text{Kn} \ll 1$, F_{ph} approaches $F_{\text{ph},s}$, and in the other limit ($\text{Kn} \gg 1$), it approaches $F_{\text{ph},f}$.

If the particle rotation cannot be neglected, there are two effects we must consider. First, the temperature gradient in the particle becomes smaller as the particle rotates faster. This effectively

reduces the asymmetry factor J_1 . In the limit of rapid rotation, the asymmetry factor J_1 approaches zero. Second, the temperature gradient generally does not coincide with the direction of the light source, that is, the radial direction. The photophoretic force has a component in the azimuthal direction and can give the particle angular momentum or take it away, depending on the orientation of the rotation. The particle drifts outward or inward, and the direction of the drift reverses when the orientation of the rotation changes. This is similar to the Yarkovsky effect acting on asteroids (Bottke et al. 2002), although in the case of photophoresis, the agents of momentum transfer are the gas molecules and not emitted photons. The particle radial drift due to this effect is stochastic if variations in the rotational orientation occur frequently before the particle travels a large distance in the radial direction. Although the study of the photophoretic Yarkovsky effect is important, we leave this for future investigations and in this paper assume that the photophoretic force is always directed in the radial direction.

For further discussion, it is convenient to normalize the radiative forces given above by the gravitational force,

$$F_{G,d} = -GMm_d/r^2, \quad (9)$$

where G is the gravitational constant, M is the mass of the central star, and m_d is the mass of the particle. We introduce a normalization factor

$$\beta = \beta_{\text{rad}} + \beta_{\text{ph}}, \quad (10)$$

where

$$\beta_{\text{rad}} = \left| \frac{F_{\text{rad}}}{F_{G,d}} \right| = \frac{3Q_{\text{rad}}L}{16\pi GMc\rho_d a}, \quad \beta_{\text{ph}} = \left| \frac{F_{\text{ph}}}{F_{G,d}} \right|. \quad (11)$$

In the free molecular regime ($\text{Kn} \gg 1$),

$$\beta_{\text{ph}} = \frac{\alpha J_1 k_B L}{16\sqrt{2}\pi GM\sigma_{\text{mol}}k_d\rho_d l(1 + 4\epsilon\sigma_{\text{SB}}T_d^3 a/k_d)}. \quad (12)$$

At large distances from the star, the dust temperature is so low that $4\epsilon\sigma_{\text{SB}}T_d^3 a/k_d \ll 1$ and β_{ph} is independent of the particle radius a .

Next we consider the forces acting on the gas. The gravity acting on a unit volume of gas is

$$F_{G,g} = -GM\rho_g/r^2, \quad (13)$$

where ρ_g is the mass density of the gas. The pressure gradient force on a unit volume is

$$F_{\nabla P} = -\frac{\partial P}{\partial r}. \quad (14)$$

We introduce a normalization factor η similarly to that for the dust particle,

$$\eta = |F_{\nabla P}/F_{G,g}|. \quad (15)$$

2.2. Gas Disk Models and Dust Parameters

For simplicity, we assume that the temperature of the gas disk, T_g , has a power-law profile in the radial direction r and is isothermal in the vertical direction z ; that is, it is written

$$T_g(r) = T_{g,0}r_{\text{AU}}^{-q}, \quad (16)$$

where the subscript zero denotes quantities at 1 AU and the non-dimensional quantity r_{AU} is the radius in AU. The gas density, ρ_g , is also assumed to have a power-law profile in r and to be in vertical hydrostatic equilibrium, that is,

$$\rho_g(r, z) = \rho_{g,0}r_{\text{AU}}^{-p_m} \exp(-\frac{1}{2}z^2/h_g^2), \quad (17)$$

where the disk scale height is $\sqrt{2}h_g$. The isothermal sound speed of the disk is $c_s = c_0r_{\text{AU}}^{-q/2}$, and h_g is written as

$$h_g(r) = c_s/\Omega_K = h_0r_{\text{AU}}^{(-q+3)/2}, \quad (18)$$

where $\Omega_K = (GM/r^3)^{1/2}$ is the Keplerian angular frequency at the disk midplane. The gas surface density is

$$\Sigma_g(r) = \int_{-\infty}^{+\infty} \rho_g dz = \sqrt{2\pi}\rho_0h_0r_{\text{AU}}^{-p}, \quad (19)$$

where $p = p_m + (q - 3)/2$. We adopt the following fiducial parameters for the central star and the gas temperature profile: $M = 1 M_{\odot}$, $L = 1 L_{\odot}$, $T_{g,0} = 278$ K, $h_0 = 3.33 \times 10^{-2}$ AU, and $q = \frac{1}{2}$. The mean mass of the gas molecules is $2.34m_{\text{H}}$, where m_{H} is the mass of a hydrogen atom (Nakagawa et al. 1986). The collisional cross section of the gas molecules is $\sigma_{\text{mol}} = 2 \times 10^{-15}$ cm² (Chapman & Cowling 1970, p. 228).

We consider disks in which most of the small dust grains have been removed and, consequently, the disks have become optically thin even in the radial direction. The dust opacity at optical wavelengths arises mainly from particles smaller than 10 μm (see Fig. 4 of Miyake & Nakagawa 1993). In order for the disk to be optically thin, the column density of small grains ($\lesssim 10 \mu\text{m}$) from the star must be smaller than 10^{-3} g cm⁻². Removal of dust grains probably occurs through coagulation of the grains into planetesimals (Weidenschilling & Cuzzi 1993; Tanaka et al. 2005; Dullemond & Dominik 2005; Nomura & Nakagawa 2006). In such disks, the gas component has likely also been reduced in amount. Indeed, most Vega-type stars do not have detectable gas components (Liseau & Artymowicz 1998; Greaves et al 2000; Coulson et al. 2004; Chen & Kamp 2004), and only a few objects have as much as several tens of Earth masses of gas. For example, HD 141569A has a gas mass of $\lesssim 60 M_{\oplus}$ (Zuckerman et al. 1995; Ardila et al. 2005). Therefore, in “model A,” we consider a disk in which the amount of gas inside 100 AU is $M_g = 2.4 \times 10^{-5} M_{\odot} = 7.9 M_{\oplus}$. (The model disk extends over 100 AU. We specify the disk mass as that inside 100 AU.) We adopt a surface density profile proposed by Hayashi et al. (1985) in which the power-law index $p = 1.5$. The gas surface density is $\Sigma_g = 1.7r_{\text{AU}}^{-1.5}$ g cm⁻². In addition to model A, we also consider a more massive disk to investigate the case in which the disk opacity due to the dust has been significantly reduced before considerable gas dissipation occurs. In “model B,” the amount of gas within 100 AU is $M_g = 1.2 \times 10^{-2} M_{\odot}$. Further, we assume a density profile that is more gradual than in model A, with $p = 0.5$. This gentle slope ensures that the gas density in the innermost part of the disk (say, ~ 0.1 AU) does not become so high that Rayleigh scattering by molecular hydrogen makes the gas disk itself become optically thick to the starlight (see § 4.1 below). The gas surface density in model B is $\Sigma_g = 25r_{\text{AU}}^{-0.5}$ g cm⁻².

For dust particles, we use the following fiducial parameters: The thermal conductivity $k_d = 10^2$ ergs s⁻¹ cm⁻¹ K⁻¹, the particle bulk density $\rho_d = 1$ g cm⁻³, the asymmetry factor $J_1 = 0.5$, the emissivity $\epsilon = 1$, and there is perfect accommodation of gas

molecules, $\alpha = 1$. The adopted value for the thermal conductivity is typical of porous aggregates (Presley & Christensen 1997). If the dust particles are more compact, the thermal conductivity can be much higher.

2.3. Radial Motion of Dust Particles

Both the radiation pressure and the photophoretic force are directed outward. If the sum of these forces is stronger than the gravity of the central star, that is, $\beta > 1$, then the particle is not bound to the central star and is ejected from the system. If $\beta < 1$, the particle is bound to the central star, but it feels a net force weaker than the gravity of the central star and its orbital motion is slower than Keplerian. Assuming the particle's orbit is circular and neglecting any contribution from the gas drag force, the azimuthal velocity of the particle is

$$v_{\theta,d} = (1 - \beta)^{1/2} v_K, \quad (20)$$

where $v_K = (GM/r)^{1/2}$ is the Keplerian velocity. The azimuthal velocity of the gas is also sub-Keplerian, because the pressure gradient force usually directs outward, and is given by

$$v_{\theta,g} = (1 - \eta)^{1/2} v_K. \quad (21)$$

Now we consider the effect of the gas drag acting on a particle that is bound to the central star (i.e., $\beta < 1$). If the particle orbits faster than the surrounding gas ($v_{\theta,d} > v_{\theta,g}$), then the drag transfers angular momentum from the particle to the surrounding gas. Consequently, the particle drifts toward the central star. From equations (20) and (21), one can see that this inward drift occurs if $\beta < \eta$. On the other hand, if the particle orbits slower than the surrounding gas ($v_{\theta,d} < v_{\theta,g}$, i.e., $\beta > \eta$), then the particle gains angular momentum from the surrounding gas and drifts away from the central star. When the particle happens to be on an orbit in which its azimuthal velocity equals the gas azimuthal velocity, there is no angular momentum transfer by gas drag, and the particle stays on the equilibrium orbit. A more detailed discussion including a derivation of the drift velocity is given by Takeuchi & Artymowicz (2001). From their equation (26) for the drift velocity, neglecting the P-R drag term $\beta_c T_s$ gives

$$v_{r,d} = \frac{\beta - \eta}{T_s + T_s^{-1}} v_K, \quad (22)$$

where the nondimensional stopping time is

$$T_s = \frac{\rho_d a v_K}{\rho_g r v_T} \quad (23)$$

(the factor of 4/3 difference between eq. [10] of Takeuchi & Artymowicz 2001 and eq. [23] above comes from different definitions of v_T ; see their eq. [6]).

We can determine the direction of the particle's radial drift by seeing whether β is larger than η . Figure 1a shows the ratio β/η plotted against the distance from the central star for model A. If a particle's β is larger than the η of the surrounding gas, it drifts away from the star, and vice versa. The ratio of radiation pressure to gravity, β_{rad} , which is inversely proportional to the particle radius a , is constant with distance from the star, r (see eq. [11]). On the other hand, as long as the gas mean free path l is larger than a (the free molecular regime), the photophoretic force is inversely proportional to the Knudsen number Kn (see eq. [4]) and hence decreases with r . Thus, at large distances from the central star, the radiation pressure dominates the photophoretic

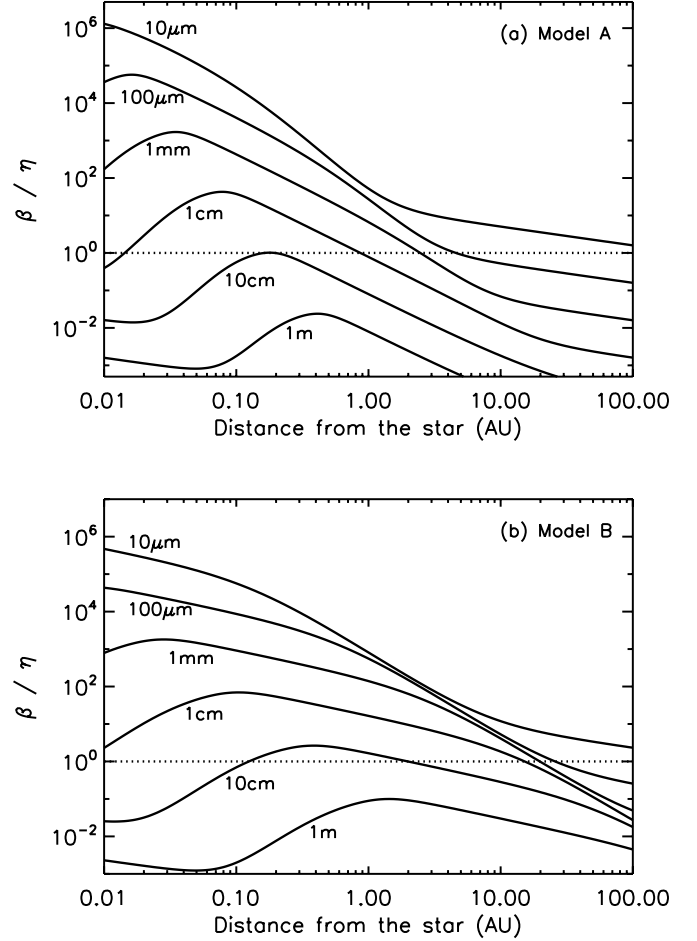


FIG. 1.—Ratio of the normalized outward force on the dust particle, β , with regard to that on the gas, η . The particle size is varied from $10 \mu\text{m}$ to 1m . The dotted lines represent $\beta = \eta$. The particles drift outward if $\beta/\eta > 1$ and drift inward if $\beta/\eta < 1$. (a) For gas disk model A ($\Sigma_g = 1.7 r_{\text{AU}}^{-1.5} \text{g cm}^{-2}$, $M_g = 2.4 \times 10^{-5} M_\odot = 7.9 M_\oplus$ inside 100AU); (b) for model B ($\Sigma_g = 25 r_{\text{AU}}^{-0.5} \text{g cm}^{-2}$, $M_g = 1.2 \times 10^{-2} M_\odot$).

force (i.e., $\beta \approx \beta_{\text{rad}}$), while at small distances, the photophoretic force dominates and $\beta \approx \beta_{\text{ph}}$. The transition occurs at 1AU for $10 \mu\text{m}$ particles, at 3AU for $100 \mu\text{m}$ particles, and at 7AU for 1mm particles. The curves in Figure 1a bend at these distances, and the slopes become gentler at larger distances. The slopes of the curves, $d(\beta/\eta)/dr$, are determined only by $d\eta/dr$ at large distances, because β_{rad} is constant with r , and have the same value for differently sized particles. Inside the transition distances, where the photophoretic force dominates, β ($\approx \beta_{\text{ph}}$) increases with decreasing Kn or decreasing distance from the central star. This increase in β continues until the mean free path of the gas molecules becomes smaller than the particle radius, that is, until Kn becomes less than unity. In the innermost part of the disk, where $\text{Kn} < 1$ (slip-flow regime photophoresis), β is proportional to Kn (see eq. [5]) and decreases with decreasing r . The transition from free molecular regime photophoresis to slip-flow regime photophoresis occurs at the distance where $\text{Kn} = 1$, and at this transition distance β/η has its maximum value. For $100 \mu\text{m}$ particles, β/η has a peak at 0.02AU , and for larger particles the peak position shifts outward. It is 0.2AU for 10cm particles.

It can be seen from Figure 1a that particles smaller than 10cm have a region where β is greater than η . In such a region the particles drift outward. The outward drift of the particles stops at the locations where $\beta = \eta$. At these locations, the particles that are drifting inward from the outer region also stop. Hence, the

particles accumulate where $\beta = \eta$ and $d(\beta/\eta)/dr < 0$, leading to the formation of a dust ring as proposed by Krauss & Wurm (2005). Particle accumulation does not occur at locations where $\beta = \eta$ but $d(\beta/\eta)/dr > 0$, because the particles drift away from such locations. Note that at the locations where particles accumulate, the Knudsen number Kn is always larger than unity, and thus the photophoretic force is expressed in the form appropriate for the free molecular regime. The location of particle accumulation is at 5 AU for 100 μm particles and moves closer to the central star as the particle radius increases. Particles of 10 cm accumulate at 0.2 AU. If the particles are larger than 10 cm, they always drift toward the central star and cannot accumulate anywhere. In sum, particle accumulation occurs if $\beta/\eta > 1$ somewhere in the disk. The accumulation location is specified by the conditions $\beta = \eta$, $d(\beta/\eta)/dr < 0$, and $\text{Kn} > 1$.

For 10 cm and 1 m particles, the curves in Figure 1a again bend at 0.02–0.05 AU. Inside these distances, the radiation pressure becomes stronger than the photophoretic force because the Knudsen number is too low. Thus, β remains constant with r in this region while η increases, resulting in a decrease in β/η .

A similar result is obtained for model B (Fig. 1b). In this model, particles of all sizes are driven farther outward compared with model A. This is because the gas density is higher in the model B disk, resulting in an increase in β_{ph} . In model B, it is also apparent that 100 μm –1 cm particles accumulate in a narrow region at 20–30 AU. This pileup of particles in a narrow ring has been pointed out by Krauss & Wurm (2005). It is a consequence of β_{ph} being independent of the particle radius at large distances (eq. [12]).

Note that the accumulation of outward-migrating particles at the ring radius does not increase the optical depth to the star. Formation of a dust ring through clearing of the inner dust disk does not suppress further evolution by photophoresis. However, after the inner dust is cleared, the optical depth of the ring increases as particles from the outer disk accumulate. When the dust ring becomes optically thick, photophoresis is weakened and then the ring shrinks. In this paper, we consider the stage in which the dust ring is optically thin.

3. PARTICLE ACCUMULATION RADIUS

As discussed in the previous section, particles accumulate at the equilibrium locations where $\beta = \eta$ and $d(\beta/\eta)/dr < 0$. In Figures 2a and 2b, the equilibrium distances for models A and B respectively are plotted as functions of the particle radius. The lines labeled “fiducial” represent the equilibrium distances calculated with the parameters given in § 2.2. The equilibrium distances for other parameters are also plotted; we vary the value of one parameter while keeping the others the same as in the fiducial model. Higher thermal conductivities $k_d = 10^5$ and 10^7 ergs $\text{s}^{-1} \text{cm}^{-1} \text{K}^{-1}$, a lower bulk density $\rho_d = 0.1 \text{ g cm}^{-3}$, a lower efficiency of photophoresis $J_1 = 0.5 \times 10^{-2}$, and a higher luminosity of the central star $L = 20 L_\odot$ are investigated. We also calculate the case in which photophoresis does not work at all ($J_1 = 0$).

3.1. Dust Concentration and Size Segregation

At the accumulation locations, photophoresis is in the free molecular regime ($\text{Kn} > 1$), and as can be seen from equation (12), β_{ph} converges to a certain value in the limit of small a . On the other hand, β_{rad} is inversely proportional to a (neglecting the size dependence of Q_{rad}), and thus radiation pressure is more efficient than photophoresis for smaller particles. In the condition $\beta = \eta$, which determines the accumulation location, β is controlled by radiation pressure for small particles and by photophoresis for

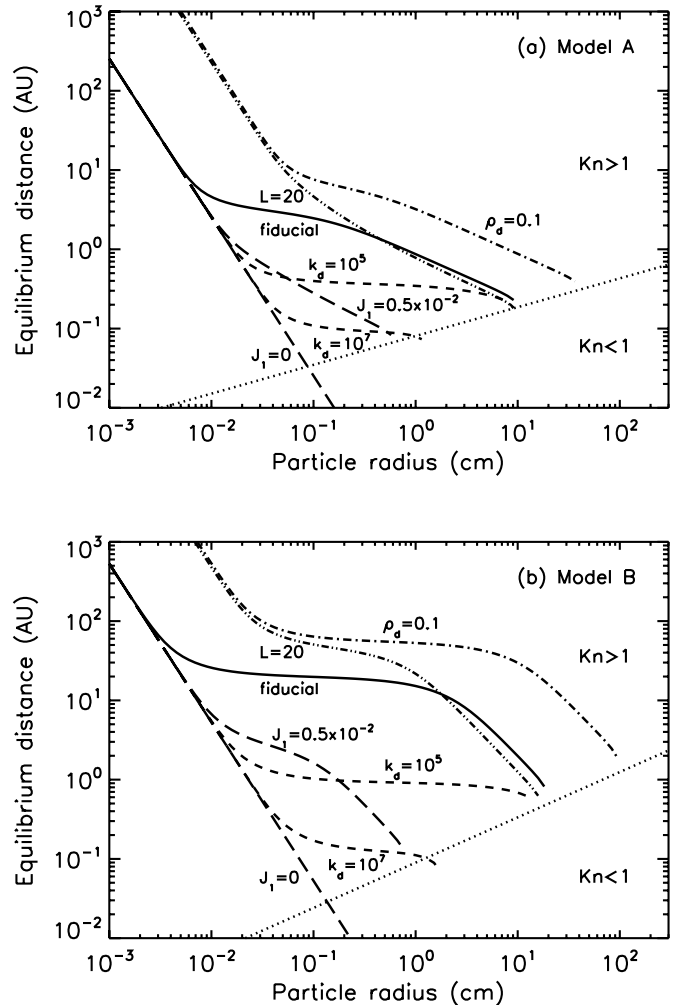


FIG. 2.—Equilibrium distances, where $\beta = \eta$, for dust particles with various physical properties: the fiducial parameters ($k_d = 10^2$ ergs $\text{s}^{-1} \text{cm}^{-1} \text{K}^{-1}$, $\rho_d = 1 \text{ g cm}^{-3}$, and $J_1 = 0.5$; solid line), higher thermal conductivity ($k_d = 10^5$ and 10^7 ergs $\text{s}^{-1} \text{cm}^{-1} \text{K}^{-1}$; short-dashed lines), smaller efficiency of photophoresis ($J_1 = 0.005$ and $J_1 = 0$; long-dashed lines), lower bulk density ($\rho_d = 0.1 \text{ g cm}^{-3}$; dot-dashed line), and a more luminous star ($L = 20 L_\odot$; double-dot-dashed line). The dotted lines show the distances where the Knudsen number is unity. Above the dotted line $\text{Kn} > 1$, and $\text{Kn} < 1$ below.

large particles. The particle size for which the transition from one behavior to the other occurs depends on the parameters that are relevant for the strength of the photophoretic force, that is, k_d and J_1 . This can be seen in Figure 2a, where the curves for different parameters depart from the straight line for $J_1 = 0$ at different particle sizes. For the fiducial dust parameters in model A (Fig. 2a, solid line), the accumulation locations for particles larger than 100 μm are controlled by photophoresis, while those of smaller particles are controlled by radiation pressure. Particles that are subject to photophoresis have a tendency to accumulate in a narrow ring region provided that all particles have the same physical properties, that is, they have the same values of ρ_d , k_d , and J_1 . For example, in the fiducial model (Fig. 2a, solid line), particles of 200 μm –2 mm accumulate in a region at 2–4 AU, and 300 μm –10 cm particles with the higher conductivity $k_d = 10^5$ ergs $\text{s}^{-1} \text{cm}^{-1} \text{K}^{-1}$ accumulate at 0.2–0.5 AU. Hence, a significant influence of photophoresis is to condense the particles of a certain size interval. For small particles, this interval is limited by the increasing influence of radiation pressure. For large particles, the limit is determined by the increasing importance of thermal emission and conduction to the gas for thermal relaxation and the

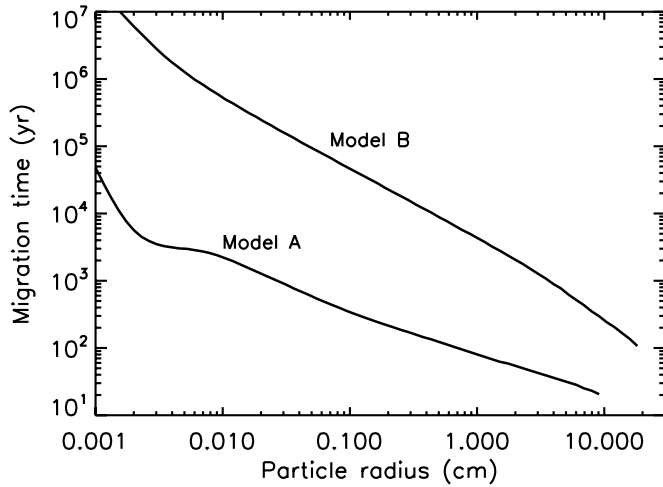


FIG. 3.— Timescales τ_{mig} for the dust particles to migrate to the accumulation locations. The dust parameters are the fiducial values.

approach to $\text{Kn} = 1$. The location of accumulation decreases with increasing thermal conductivity. Thus, particles with different thermal properties can be separated in the disk by this process. While $k_d = 10^2 \text{ ergs s}^{-1} \text{ cm}^{-1} \text{ K}^{-1}$ corresponds to very porous dust aggregates, values around $10^5 \text{ ergs s}^{-1} \text{ cm}^{-1} \text{ K}^{-1}$ are appropriate for compact rocky or glassy grains, and $k_d = 10^7 \text{ ergs s}^{-1} \text{ cm}^{-1} \text{ K}^{-1}$ for purely metallic particles. As discussed by Wurm & Krauss (2006), compact particles such as chondrules or CAIs might have accumulated in the region of the asteroid belt whereas porous dust aggregates were driven farther outward by photophoresis in the forming solar system (see Fig. 2*b* for a disk model as massive as the solar nebula).

In actual disks, the properties of particles are probably not homogeneous, with the dust disks being composed of a wide variety of particles. Even particles of the same size therefore spread over a certain range of distances, and a dust ring formed by photophoresis will have some extent in the radial direction. We still expect, however, particle concentration in the disk to happen to some degree. Even with a range of particle properties as wide as that considered in Figure 2*a*, we clearly see two populations of dust particles. All the particles at distances greater than 10 AU are smaller than 1 mm and do not show any sign of concentration. The dust population inside 10 AU is composed of particles larger than $100 \mu\text{m}$ and is confined in a region between 0.1 and 10 AU. We refer to this region as the inner disk. These two populations are divided based on whether the radiation pressure or the photophoretic force is larger. The population of small particles is subject to radiation pressure, and the other is subject to photophoresis. Hence, the effect of photophoresis is to discriminate large particles from small particles and to confine them to the inner region of the disk.

3.2. Inner Holes

Another significant feature of Figure 2*a* is that in the region below the dotted line, which represents the area where $\text{Kn} < 1$, there is no equilibrium location where particle accumulation through photophoresis occurs. As discussed in § 2.3, particle accumulation by photophoresis always occurs at locations where $\text{Kn} > 1$. If photophoresis does not work ($J_1 = 0$), it can be seen from Figure 2*a* that particles can accumulate even in the region where $\text{Kn} < 1$. This feature represents a possible observational criterion to show whether photophoresis actually occurs in gas disks, although it requires observations of the innermost part of the disk ($r \lesssim 0.1 \text{ AU}$) with very high spatial resolution. If photophoresis

actually works, one would find that an inner hole opens in the dust disk, and that its radius is determined by the condition $\text{Kn} = 1$. If photophoresis does not work, on the other hand, dust particles would exist even in regions where $\text{Kn} < 1$. An actual dust disk is a mixture of particles with various physical properties. If the dust particles have the range of properties considered in Figure 2, the inner radius (which is determined by the particles with $k_d = 10^7 \text{ ergs s}^{-1} \text{ cm}^{-1} \text{ K}^{-1}$ or $J_1 = 0.5 \times 10^{-2}$) is $\sim 0.1 \text{ AU}$. This inner radius may be as small as 0.03 AU, if there are considerable numbers of particles upon which photophoresis works very weakly (i.e., particles of very small J_1 , but in that case the inner disk clearing would probably be suppressed, as shown by the $J_1 = 0$ line.)

We stress that the Knudsen number Kn is a function only of the dust particle size a and the mean free path of the gas molecules l . Thus, the inner radii of dust disks do not directly reflect the dust particles' physical properties, such as the thermal conductivity k_d , the bulk density ρ_d , and the efficiency of photophoresis J_1 . (The particle size at the inner edge does depend on the particle properties.) The fact that the inner radius of the dust disk is determined only by the particle size will be of considerable help in observationally testing the idea of inner hole opening by photophoresis. On the other hand, it is of great importance to have an independent measurement of the local gas density to decide whether the condition $\text{Kn} = 1$ is fulfilled, which might still be a challenging task with modern observational techniques.

3.3. Massive Disks

Figure 2*b* shows the equilibrium distances for the same parameter combinations as in Figure 2*a*, but for disk model B. In this model, where the disk mass (inside 100 AU) is 500 times larger than that of model A, 1 mm–10 cm particles may extend farther from the central star than in model A as a result of photophoresis (up to $\sim 100 \text{ AU}$). The inner radius of the dust disk locates at $\sim 0.1 \text{ AU}$ (for particles with $k_d = 10^7 \text{ ergs s}^{-1} \text{ cm}^{-1} \text{ K}^{-1}$ or $J_1 = 0.5 \times 10^{-2}$), similar to that in model A. This is just because we adopted a density distribution for model B such that the distances where Kn equals unity for particle sizes a between 1 mm and 1 m do not considerably differ from those in model A. This choice of density distribution comes from the requirement that the gas disk must be optically thin, and we take a marginally optically thin disk (see § 4.1 below).

3.4. Timescale of Structure Formation

The timescale for the dust particles to migrate to the accumulation locations is $\tau_{\text{mig}} = |r_{\text{eq}}/v_{r,d}|$, where r_{eq} is the equilibrium distance shown in Figure 2 and $v_{r,d}$ is the radial drift velocity. In equation (22), $\beta \sim \eta$ near this equilibrium distance, and thus the drift velocity is estimated as $v_{r,d} \sim \eta v_K / (T_s + T_s^{-1})$. The migration timescale is then $\tau_{\text{mig}} \sim (T_s + T_s^{-1}) / (\eta \Omega_K)$, where the value is calculated at r_{eq} . Figure 3 shows the migration timescales for the fiducial dust parameters of models A and B. For both, the timescales are shorter than 10^6 – 10^7 yr , which is the expected age of the transitional disks, except for small particles ($a \lesssim 100 \mu\text{m}$) in model B. Hence, the disk structure and the inner hole are expected to form quickly once a disk becomes transparent to the starlight. (In disks more tenuous than model A, photophoresis effectively works only in the dense innermost part of the disk, and thus the dust accumulation location approaches the star. For example, in a disk 10^{-3} times as tenuous as model A, that is, in a disk with $M_g \sim 10^{-2} M_{\oplus}$, particle accumulation occurs only inside 0.1 AU. The migration timescale for $100 \mu\text{m}$ –1 cm particles at $\lesssim 0.1 \text{ AU}$ is still less than 10^4 yr .)

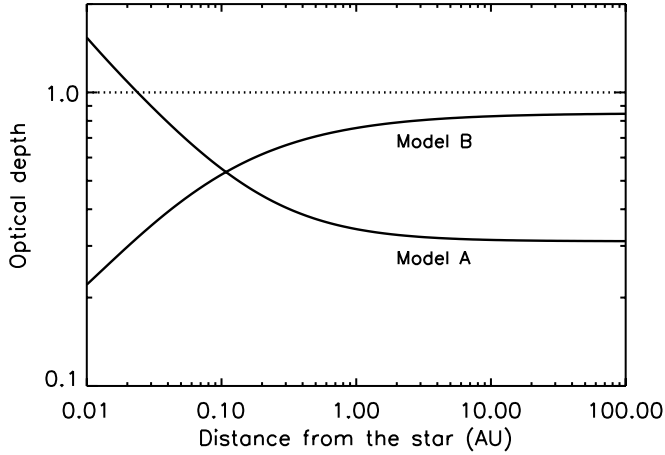


FIG. 4.—Optical depth τ_{H_2} due to Rayleigh scattering of H_2 from the typical point of the star ($0, 0.424R_*$) to the midplane of the disk at $(r, 0)$. The dotted line represents $\tau_{\text{H}_2} = 1$.

The migration timescale in Figure 3 is much shorter than the orbital decay time due to Poynting-Robertson drag. For example, $100 \mu\text{m}$ particles in model A accumulate at 4 AU in $\tau_{\text{mig}} = 2 \times 10^3 \text{ yr}$. The particles have $\beta_{\text{rad}} = 6 \times 10^{-3}$ and the timescale due to P-R drag is $\tau_{\text{PR}} = 400[r/(1 \text{ AU})]^2 \beta_{\text{rad}}^{-1} \text{ yr} = 10^6 \text{ yr}$ (Burns et al. 1979), much longer than τ_{mig} . In both model A and model B, it is found that $\tau_{\text{mig}} \ll \tau_{\text{PR}}$ for any particle size. This means that P-R drag is much weaker than gas drag and can be neglected.

4. OPACITY OF THE DISK GAS

In the previous sections, we assumed the disk to be optically thin even in the radial direction and that dust particles directly receive the light from the central star. This assumption requires that both the dust and gas opacities of the disk be sufficiently small. It applies to a stage in which most of the dust grains are packed together into planetesimals or larger objects and the disk opacity due to the dust has become negligible. Such a situation has probably been realized in some Vega-type stars. The gas disk also must be transparent, although photophoresis requires a certain amount of gas. In this section, we discuss whether a gas disk that is dense enough for photophoresis to work is transparent to the starlight.

We assume that the gas disk is mostly composed of hydrogen molecules. Thus, Rayleigh scattering by H_2 is a possible and probably dominant mechanism of light extinction in the disk. In § 4.1, we consider the gas opacity due to Rayleigh scattering by H_2 and estimate the maximum gas density at which the gas disk is marginally opaque to the light of the central star. Our estimate gives a lower limit on the gas opacity, because only Rayleigh scattering by H_2 is taken into account, and thus the derived maximum gas density should be considered an upper limit. A transparent gas disk in which photophoresis works must be less dense than our estimate. If other extinction mechanisms work more effectively than Rayleigh scattering by H_2 , this upper density limit becomes smaller. In § 4.2, we briefly discuss other extinction mechanisms.

4.1. Rayleigh Scattering by Hydrogen Molecules

The cross section for Rayleigh scattering by H_2 per molecule is

$$\sigma_{\text{H}_2} = 8.4909 \times 10^{-29} \left(\frac{\lambda}{1 \mu\text{m}} \right)^{-4} \text{ cm}^2, \quad (24)$$

where λ is the wavelength of the light (Tsuji 1966). In this subsection, we make an order-of-magnitude argument and simply

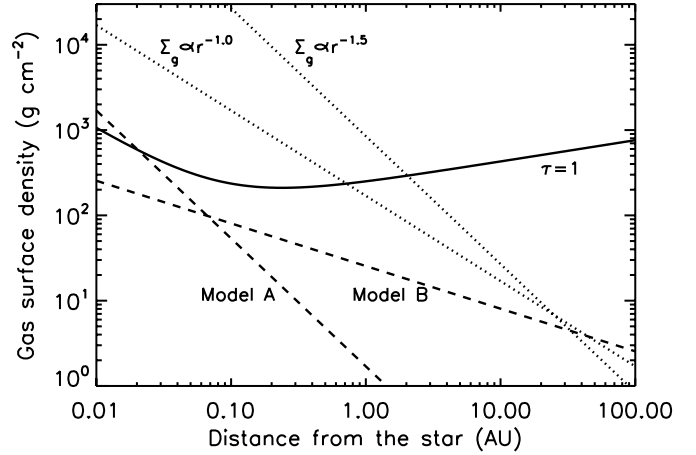


FIG. 5.—Comparison of the density profiles for models A and B (*dashed lines*) with the maximum gas density required to be optically thin to the central star (*solid line*). The dotted lines show density profiles that have the same amount of mass as model B (inside 100 AU) but different slopes ($\Sigma_g \propto r^{-1.5}$ and $\Sigma_g \propto r^{-1.0}$).

estimate the opacity around the central wavelength of the central star's spectrum, $\lambda = 0.5 \mu\text{m}$. The stellar light source is represented as point sources located slightly above and beneath the origin, $z_* = \pm 0.424R_*$, where R_* is the radius of the central star (Hollenbach et al. 1994) and we assume $R_* = 1.0 R_\odot$. The optical depth from the star, at $(0, z_*)$, to a dust particle on the midplane, $(r, 0)$, is

$$\tau_{\text{H}_2} = \int \sigma_{\text{H}_2} n_g ds, \quad (25)$$

where n_g is the number density of the gas molecules (we assume that all the gas is composed of H_2 , for simplicity).

Figure 4 shows the optical depth from the central star as a function of the distance r . In both models A and B, the disk is optically thin (except at $r < 0.03 \text{ AU}$ in model A). Note that the disk mass (within 100 AU) in model B is 500 times larger than that in model A, but the optical depths from the star are not much different. This is because the opacities of the disks are mainly determined by the density at $\sim 0.1 \text{ AU}$, and the densities at 0.1 AU in models A and B do not differ much (Fig. 5). The starlight that illuminates a particle located at a distance $r \gg 0.1 \text{ AU}$ gets into the disk at a distance $\sim 0.1 \text{ AU}$, because the disk scale height at 0.1 AU is $\sqrt{2}h_g \approx 2 \times 10^{-3} \text{ AU} \approx 0.4R_* \approx z_*$. Model B has the density profile $\Sigma_g \propto r^{-0.5}$ and most of the gas mass is distributed in the outermost part of the disk, while the density profile of model A is more steep ($\Sigma_g \propto r^{-1.5}$) and the disk mass is more concentrated in the innermost region. Thus, even though the disk mass of model B is 500 times larger than that of model A, the densities at 0.1 AU in model A and B are similar. For particles located much farther out than 0.1 AU , the optical depth from the central star does not change with r .

For particles inside $\sim 0.1 \text{ AU}$, the location where the starlight enters the disk moves toward the central star as the particle position gets closer to the star. In model A, the optical depth is determined by the gas density at the point where the starlight enters the disk, which rapidly increases with decreasing distance r . Consequently, the optical depth increases with decreasing particle distance. In model B, the concentration of gas in the innermost part of the disk is moderate. Thus, the decrease in the path length of the starlight (which is approximately proportional to r) dominates the increase in the gas density where the starlight enters the disk. The optical depth from the star decreases with decreasing particle distance in model B.

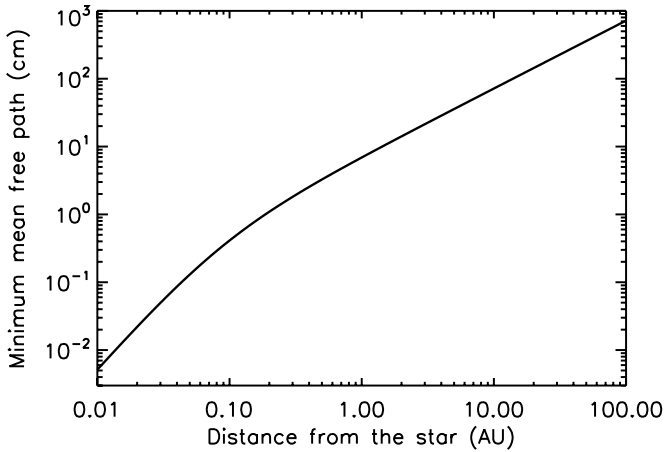


FIG. 6.— Mean free path of the hydrogen molecules in the critical disk, where the optical depth to the central star is unity.

We next estimate the maximum gas density of a disk for it to be optically thin. The optical depth to the star from $(r, 0)$ at the disk midplane is estimated as $\tau \approx \sigma_{\text{H}_2} n_g s$, where the number density of hydrogen molecules n_g is estimated at $(r, 0)$ and s is the path length of the starlight. The path length is the distance between $(r, 0)$ and the point where the starlight enters the disk. The location of the latter point is approximately calculated as the point where the line connecting $(0, 0)$ and $(r, \sqrt{2}h_g)$ crosses the line connecting $(0, z_*)$ and $(r, 0)$. The condition $\tau < 1$ reduces to the condition for the gas surface density $\Sigma_g < \sqrt{2\pi} h_g m_{\text{H}_2} / (\sigma_{\text{H}_2} s)$, where m_{H_2} is the mass of a hydrogen molecule. The solid line in Figure 5 shows the upper limit on the gas surface density for the optical depth to the star to be less than unity. We see that for $r > 0.02$ AU, the surface densities of both model A and model B (dashed lines) are less than the critical density for $\tau = 1$ (solid line). For comparison, the surface densities of disks having the same amount of mass as model B (inside 100 AU) but different slopes in the density distribution are shown ($\Sigma_g \propto r^{-1.5}$ and $\Sigma_g \propto r^{-1.0}$; dotted lines). It can be seen that if the disk is centrally concentrated, the disk is optically thick in the inner region of the disk.

The condition $\tau < 1$ reduces also to a condition for the mean free path of the gas molecules. The mean free path of the gas must be larger than the value shown in Figure 6 for the disk to be optically thin. This minimum value is also interpreted as the minimum size of dust particles that compose the inner edge of the dust disk, because the location of the inner edge is determined by the condition $\text{Kn} = 1$. Thus, in order to observationally test whether an inner hole is produced by photophoresis, we would have to detect particle accumulation of sizes larger than the value indicated in Figure 6. Suppose that, for example, a dust disk has an inner hole of radius 0.04 AU. If this inner hole was formed by photophoresis, the gas disk at 0.04 AU must be optically thin, and from Figure 6, the mean free path at 0.04 AU must be larger than 1 mm. Because only particles larger than the mean free path can accumulate through photophoresis, the particles at the inner edge must be larger than 1 mm. This minimum particle size becomes larger as the inner radius of the dust disk becomes larger. If the inner radius is 1 AU, the particle size must be greater than 10 cm.

4.2. Other Opacity Sources

1. *Bound-free and free-free absorption of negative hydrogen ions.*—The cross section for bound-free and free-free absorption is proportional to the electron pressure. Thus, this absorption works

in environments where the ionization degree is high and would be efficient only in the innermost regions of the disk, provided the disk gas is thermally ionized. In both models A and B, the temperature at 0.02 AU is $T \approx 2000$ K, and the gas pressure is $P_{\text{H}_2} \sim 10^3$ dyn cm $^{-2}$ (the molecular hydrogen dominates the gas pressure). The partial pressures of electrons and hydrogen atoms are $P_e/P_{\text{H}_2} \sim 10^{-7}$ and $P_{\text{H}}/P_{\text{H}_2} \sim 3 \times 10^{-2}$, respectively (see Fig. 1 of Tsuji 1966; solar abundance is assumed). At the optical wavelength $\lambda = 0.5$ μm , the bound-free absorption dominates the free-free absorption, and the absorption cross section per hydrogen molecule is $\sigma_{\text{H}^-, \text{bf+ff}} \sim 10^{-23} P_e P_{\text{H}} / P_{\text{H}_2}$ cm 4 dyn $^{-1} \sim 3 \times 10^{-29}$ cm 2 , where we used the value from Table 2 of Tsuji (1966). Since the cross section of bound-free absorption sensitively depends on λ and T , we took the highest value around $\lambda \approx 0.5$ μm and $T \approx 2000$ K in Tsuji's table as representative (we take the value for $\lambda = 0.5$ μm and $T = 1938$ K). From equation (24), the cross section for Rayleigh scattering at $\lambda = 0.5$ μm is $\sigma_{\text{H}_2} = 1.36 \times 10^{-27}$ cm 2 . The cross section for bound-free and free-free absorption is much smaller than that for Rayleigh scattering even at the innermost part ($r = 0.02$ AU) of disk models A and B and thus can be ignored. (Recall that stellar photons penetrate the disk at ~ 0.1 AU for calculating the optical depth to $r \gg 0.1$ AU.)

2. *Free-free absorption of negative hydrogen molecules.*—This absorption works only at the innermost part of the disks. Thus, we estimate the cross section at 0.02 AU for the model disks, which is $\sigma_{\text{H}^-, \text{ff}} \sim 10^{-27} P_e$ cm 4 dyn $^{-1} \sim 10^{-31}$ cm 2 , where we used equation (8) of Tsuji (1966). This value is much smaller than that for Rayleigh scattering, and free-free absorption of negative hydrogen molecules can be ignored.

3. *Collision-induced absorption of hydrogen molecules.*—This works efficiently if the gas pressure is high. The cross section is expressed as $\sigma_{\text{CIA}} = k_{\text{CIA}} n_g / n_{\text{L}}^2$, where k_{CIA} is the opacity in units of cm $^{-1}$ amagat $^{-2}$ and $n_{\text{L}} = 2.69 \times 10^{19}$ cm $^{-3}$ is Loschmidt's number. We consider the innermost part of the disk. The gas number density at 0.02 AU in models A and B is $n_g \sim 10^{16}$ cm $^{-3}$. At the optical wavelength $\lambda = 0.5$ μm , the opacity k_{CIA} due to H $_2$ -H $_2$ and H $_2$ -He collisions is less than 10^{-11} cm $^{-1}$ amagat $^{-2}$ as long as $T < 4000$ K (see Figs. 1 and 2 of Borysow et al. 1997). Thus, σ_{CIA} is smaller than 10^{-34} cm 2 and can be ignored in comparison with Rayleigh scattering.

4. *Thomson scattering.*—The cross section for Thomson scattering per hydrogen molecule is $\sigma_e = 6.65 \times 10^{-25} P_e / P_{\text{H}_2}$ cm 2 . This can be ignored compared with Rayleigh scattering, as long as $P_e / P_{\text{H}_2} \ll 10^{-3}$.

5. *Molecular absorption bands.*—In the innermost part of the disk, where the temperature is high enough to vaporize refractory elements from the dust, gas molecules such as TiO and VO contribute to the gas opacity at optical wavelengths (Tsuji 1971; Alexander & Ferguson 1994; Ferguson et al. 2005). The rotation-vibration lines of such molecules overlap and create a band structure veiling the optical wavelengths. We calculated the gas opacity of disk models A and B due to the molecular absorption bands. In the calculation, we used the code developed by Tsuji (2002) for calculating the opacity of cool stellar atmospheres and assumed solar abundances for the gas and dust mixture. At optical wavelengths ($\lambda \approx 0.5$ μm), absorption by VO becomes stronger than Rayleigh scattering of H $_2$ for $T > 1300$ K, and absorption by TiO becomes stronger for $T > 1400$ K. Thus, in the disk within 0.05 AU of models A and B, where the temperature is higher than 1300 K, the gas opacity is dominated by the molecular absorption bands. Our estimate of the gas opacity in § 4.1 is not appropriate for the gas inside 0.05 AU. For dust particles at $r \gg 0.1$ AU, the rays from the central star enter the disk at ~ 0.1 AU, where the gas opacity is dominated by Rayleigh scattering, and the contribution of the

molecular absorption bands can be neglected. Most of the refractory elements may be confined in large bodies such as planetesimals and be removed from the gas phase. In such cases, the contribution of the molecular absorption bands is reduced.

5. DISCUSSION AND SUMMARY

5.1. Thermal Relaxation and Rotation Times of Dust Particles

As mentioned in § 2.1, if particles rotate rapidly, photophoresis does not work. Even if particle rotation is not considerably rapid compared with the thermal relaxation time of the particle, the photophoretic Yarkovsky effect may prevent particle accumulation. Such cases in which photophoresis does not work are represented by the model with $J_1 = 0$, in which the incident starlight does not cause any temperature gradient in the particles. If photophoresis is suppressed for any reason, particles can reside in the region where $\text{Kn} < 1$ (Fig. 2), and such cases can be observationally distinguished from disks in which photophoresis has cleared the dust in the innermost region. Hence, whether particles in gas disks rotate rapidly or not can be observationally investigated by checking whether dust in the region with $\text{Kn} < 1$ is cleared or not.

In this subsection, we estimate the thermal relaxation time of a dust particle and then compare it with the rotation period induced by gas turbulence or by photophoresis itself. We use a simple model of a cylindrical dust particle, described in Appendix A. Consider such a dust particle with radius a and height $2a$ (see Fig. 9 below). The stellar radiation flux I irradiates the front surface. We suppose that at the beginning, the temperature inside the particle is homogeneous. This initial (or average) temperature T_d is given by equation (A14), assuming that the incident flux I balances the thermal radiation from the front and back surfaces. (Radiation from the side surface is ignored for simplicity.) The temperature of the front surface increases to an equilibrium value T_f in a thermal relaxation time τ_{th} . During this time, the incident energy at the front surface conducts for a length δa and forms a skin layer of temperature gradient. During τ_{th} , the temperature at the front surface is approximated as the initial value T_d and the energy flux inside the skin layer is estimated as $Q_{\text{con}} \approx I - \sigma_{\text{SB}} T_d^4 = I/2$. (We set $\epsilon = 1$.) When the depth of the skin layer has grown to δa and the temperature of the front surface converges to T_f , the energy flux is $Q_{\text{con}} \approx k_d(T_f - T_d)/\delta a$. Equating these two expressions for Q_{con} , the thickness of the temperature gradient layer is

$$\delta a = 2k_d T_d \Delta / I, \quad (26)$$

where $\Delta = (T_f - T_d)/T_d$. Note that the maximum value of δa is $2a$. The thermal relaxation time is

$$\tau_{\text{th}} = c_d \rho_d \delta a^2 / k_d, \quad (27)$$

where c_d is the specific heat capacity of the particle.

Figure 7 shows τ_{th} for $10 \mu\text{m}$ – 10 cm particles in the disk of model A. We set the particle bulk density $\rho_d = 1 \text{ g cm}^{-3}$, the specific heat capacity $c_d = 10^7 \text{ ergs g}^{-1} \text{ K}^{-1}$, and the thermal conductivity $k_d = 10^2 \text{ ergs s}^{-1} \text{ cm}^{-1} \text{ K}^{-1}$. The temperature difference Δ is calculated from equation (A15). At small distances from the star, radiative cooling, $4\epsilon\sigma_{\text{SB}}T_d^4$, dominates in determining Δ in equation (A15), and $\Delta \approx \frac{1}{4}$. Thus, τ_{th} is independent of the particle size a and is proportional to T_d^{-6} . In our model $T_d \propto r^{-1/2}$, and thus $\tau_{\text{th}} \propto r^3$. At large distances, on the other hand, internal thermal conduction $k_d T_d/a$ determines Δ . In this case, the skin depth is $\delta a = a$. Hence, τ_{th} is proportional to a^2 and independent of r .

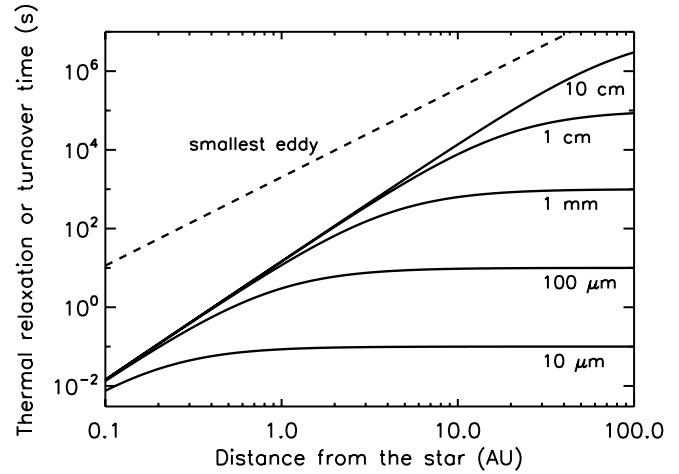


FIG. 7.—Thermal relaxation times of cylindrical particles of various sizes (solid lines) vs. distance from the star. The dashed line shows the turnover time, τ_{ed} , of the smallest eddies for $\alpha_{\text{tur}} = 10^{-2}$.

If the rotation period of the particle is smaller than τ_{th} , photophoresis is considerably suppressed. Particle rotation can be excited by several mechanisms, such as Brownian motion, gas turbulent motion, and collisions with other dust particles, and the photophoretic force itself can induce rotation if it has an offset from the mass center. Detailed calculation of the rotation period for each mechanism is beyond the scope of this paper. Here we make a rough estimate of the rotation speed induced by turbulence and by the photophoretic force.

Suppose that the gas disk has isotropic turbulence with a Kolmogorov energy spectrum. We assume that the largest eddies have size $L = \alpha_{\text{tur}}^{1/2} h_g$ and velocity $V = \alpha_{\text{tur}}^{1/2} c_s$, where α_{tur} is the “ α -viscosity” parameter (Cuzzi et al. 2001). The energy of turbulent motion cascades down to smaller eddies and finally dissipates as a result of the molecular viscosity. From dimensional analysis, the energy dissipation rate per unit mass is $\dot{\epsilon} \sim V^3/L \sim \alpha_{\text{tur}} c_s^2 \Omega_K$. The eddy turnover time is faster for smaller eddies, and that for the smallest eddies is

$$\tau_{\text{ed}} \sim \left(\frac{\eta_{\text{vis}}}{\rho_g \dot{\epsilon}} \right)^{1/2} \sim \alpha_{\text{tur}}^{-1/2} \left(\frac{l}{h_g} \right)^{1/2} \Omega_K^{-1}, \quad (28)$$

where $\eta_{\text{vis}} = l v_T \rho_g / 2$ is the molecular viscosity (Weidenschilling 1984). The smallest eddies can induce a particle rotation period as short as τ_{ed} if the particle is well coupled to the turbulent motion of the smallest eddies. However, if the particle does not strongly couple to the gas, the rotation period will be longer than τ_{ed} . In Figure 7, the turnover time, τ_{ed} , of the smallest eddies is plotted by the dashed line for $\alpha_{\text{tur}} = 10^{-2}$. The particle rotation period induced by gas turbulence is expected to lie above the dashed line and therefore is much longer than the thermal relaxation time.

We next consider rotation induced by the torque exerted by photophoresis. Consider again a cylindrical dust particle and suppose that the photophoretic force is exerted on a point at a distance b from the cylinder axis. The torque is $K = bF_{\text{ph}}$. The value of b is unknown, and we treat it as a free parameter. The principal moment of inertia of the cylinder (for the axis perpendicular to the cylinder axis) is $I_{\text{xx}} = 7\pi a^5 \rho_d / 6$. The time needed for an initially stationary particle to rotate 180° is

$$\tau_{\text{rot}} = \left(\frac{2\pi I_{\text{xx}}}{K} \right)^{1/2} = \left(\frac{7\pi^2 \rho_d a^5}{3bF_{\text{ph}}} \right)^{1/2}. \quad (29)$$

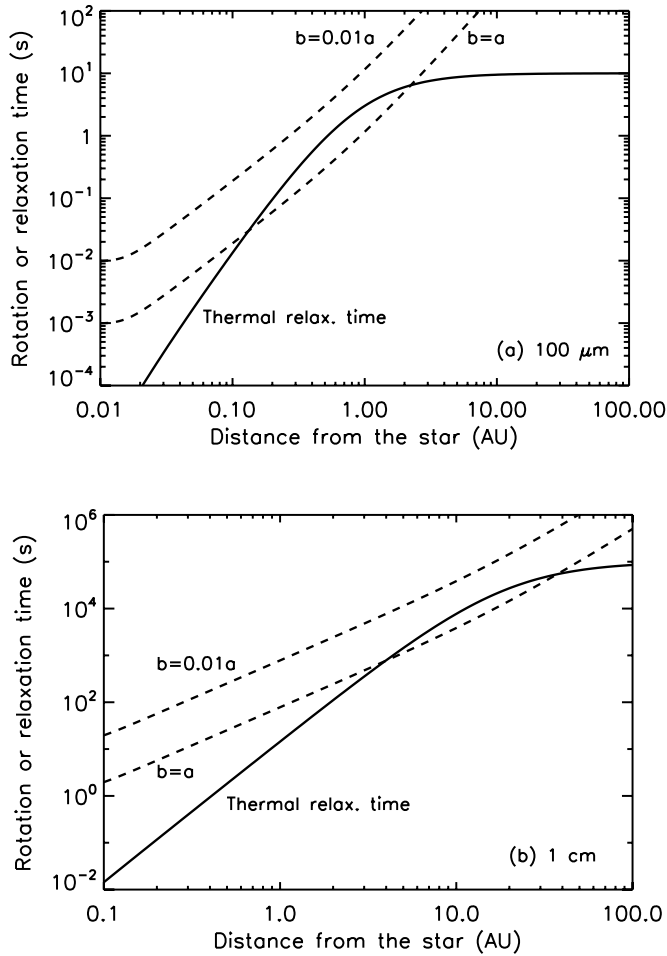


FIG. 8.—Times taken for a particle to rotate 180° by photophoresis (*dashed lines*) for (a) $100\ \mu\text{m}$ particles and (b) $1\ \text{cm}$ particles. The photophoretic force is exerted on a point at a distance $b = a$ or $b = 0.01a$ from the cylinder axis. The solid lines show the thermal relaxation time.

In Figure 8, the rotation time τ_{rot} is plotted for assumed offsets $b = a$ and $b = 0.01a$. If the photophoretic force is applied at a large offset ($b = a$), the rotation time can be shorter than the thermal relaxation time at $0.1\text{--}2\ \text{AU}$ for $100\ \mu\text{m}$ particles and that at $4\text{--}40\ \text{AU}$ for $1\ \text{cm}$ particles. In such regions, photophoresis is probably significantly suppressed. In order for photophoresis to work effectively in the whole disk, the off-center of the photophoretic force has to be as small as $b = 0.01a$.

5.2. Characteristic Structure Due to Photophoresis

The dust disk structure created by photophoresis has three zones: the outer disk, the inner disk, and the inner hole. The outer disk is composed of small ($a \lesssim 1\ \text{mm}$, or $\beta \gtrsim 0.01$) particles, and their dynamics is controlled mainly by radiation pressure. The inner disk is composed of large ($a \gtrsim 100\ \mu\text{m}$, or $\beta \lesssim 0.01$) particles accumulating there as a result of photophoresis. The boundary between the outer and inner regions is at $10\text{--}100\ \text{AU}$, depending on the gas density profile. The inner hole opens inside $\sim 0.1\ \text{AU}$, where the Knudsen number Kn is smaller than unity for the particles that photophoresis works on effectively ($a = 100\ \mu\text{m}\text{--}10\ \text{cm}$).

The structure formed by photophoresis should be compared with the structure of gas-free disks. Modeling of gas-free dust disks also shows zonal structure that consists of an outer extended disk, an inner disk, and an inner hole (Thébault & Augereau 2005; Wyatt 2006; Strubbe & Chiang 2006; Krivov et al. 2006). In these models, a planetesimal belt is assumed to exist and dust

particles are continuously produced by planetesimal collisions. The inner disk is composed of large particles whose orbits are hardly affected by radiation pressure and are nearly circular. Thus, the location and width of the inner disk are basically similar to those of the planetesimal belt. The outer disk extends beyond the planetesimal belt and is composed of small particles whose β -value is large. Their orbits are strongly influenced by radiation pressure and are excited to high eccentricities. In the model of Thébault & Augereau (2005), the particles of the outer disk have $\beta > 0.05$, which is relatively large compared with the β of our models. In our models, the particles' β in the outer disk can be as small as 0.01. Therefore, infrared-to-millimeter radio observations of outer disks and determination of the particle size will provide key information for determining which model is plausible.

Our models of photophoresis also predict that an inner hole opens in the dust disk, but the gas still fills the hole. This is a significant feature, but it is difficult to test this with the present observational techniques. It is necessary to observe the gas, but the amount of gas in optically thin disks is probably quite small, and most Vega-type stars do not have gas in an amount exceeding the current detection limits. Furthermore, the radius of the inner hole is on the order of $0.1\ \text{AU}$, and the temperature there is close to the sublimation temperature of the dust. (The temperature exceeds $1500\ \text{K}$ inside $0.03\ \text{AU}$ in our model disks.) Therefore, what is needed is a careful observation that can distinguish between inner holes created by photophoresis and those created by dust sublimation.

5.3. Summary

We have studied dust accumulation by photophoresis, using formulae for the photophoretic force that are applicable to the free molecular regime and to the slip-flow regime. The main results are as follows:

1. Particle accumulation occurs at a point where the outward acceleration on the gas due to the pressure gradient equals the outward acceleration on the particles due to radiation pressure and photophoresis.
2. Photophoresis creates an inner disk composed of relatively large particles ($a = 100\ \mu\text{m}\text{--}10\ \text{cm}$). The inner disk extends from $0.1\ \text{AU}$ to $10\text{--}100\ \text{AU}$ and is surrounded by an outer disk composed of small particles ($a \lesssim 1\ \text{mm}$).
3. An inner hole opens inside $\sim 0.1\ \text{AU}$. Its radius is determined by the condition $\text{Kn} = 1$ for the maximum size particles that photophoresis effectively works on ($a = 100\ \mu\text{m}\text{--}10\ \text{cm}$).

Photophoresis works effectively only when the disk is optically thin. Most small ($\lesssim 10\ \mu\text{m}$) dust grains must be removed from the disk such that their column density to the star becomes smaller than $10^{-3}\ \text{g cm}^{-2}$. For example, at $1\ \text{AU}$ the dust density must be less than $10^{-16}\ \text{g cm}^{-3}$, that is, 10^{-5} times smaller than the value of the minimum-mass solar nebula model (Hayashi et al. 1985). The gas disk also must be optically thin. Figure 5 shows that the gas surface density must be smaller than $10^2\text{--}10^3\ \text{g cm}^{-2}$. At $0.1\ \text{AU}$, where the typical ray from the star enters the disk (for the dust particles at $r \gg 0.1\ \text{AU}$), this value is $\sim 10^{-2}$ times as small as the value of the minimum-mass solar nebula model (Hayashi et al. 1985). Even in such a tenuous gas disk, the photophoretic force is strong enough to change the dust disk structure inside a few AU, as shown by model A (Fig. 2a). If the gas density is more tenuous than in model A, the region where photophoresis has a substantial effect shrinks toward the central star. In a gas disk with $\frac{1}{10}$ the gas density of model A, photophoresis on millimeter-sized particles works effectively only

within 1 AU, and in a disk with 10^{-2} times the gas density, the effective region shrinks to 0.3 AU.

We thank Ingrid Mann, Tadashi Mukai, Yoichi Itoh, and Yoshitsugu Nakagawa for useful discussions. We are grateful to Takashi Tsuji for extensive and helpful discussions and for kindly providing his numerical code to calculate the gas opacity. We are

grateful to anonymous referees for their constructive comments. This work was supported by the 21st Century Center of Excellence program “The Origin and Evolution of Planetary Systems” of the Ministry of Education, Culture, Sports, Science and Technology of Japan (MEXT) and also by Grants-in-Aid for Scientific Research 17740107 and 17039009 from MEXT. O. K. is grateful to Gerhard Wurm and acknowledges the support of the Deutsche Forschungsgemeinschaft.

APPENDIX A

A SIMPLE ESTIMATE OF THE PHOTOPHORETIC FORCE

In this appendix, we estimate the magnitude of the photophoretic force using a simple calculation. We consider a cylindrical dust particle with radius a and height $2a$ (see Fig. 9). The particle is surrounded by gas of temperature T_g . In general, T_g differs from the average temperature of the particle, T_d . In deriving the photophoretic force below, we assume $T_g = T_d$ and consider cases with $T_g \neq T_d$ later. The incident radiation flux, I , is parallel to the cylinder axis (z -axis) and irradiates the front surface. The temperature at the front surface increases to T_f , and it radiates an energy flux $\epsilon\sigma_{\text{SB}}T_f^4$, where ϵ is the emissivity. Some of the incident energy is conducted to the gas at a rate q_f per unit area, and the residual energy flows to the back surface at a rate Q_{con} per unit area. For simplicity, we ignore the energy transfer through the side surface. The temperature of the back surface is T_b . The back surface radiates energy flux $\epsilon\sigma_{\text{SB}}T_b^4$ and conducts heat to the gas at a rate q_b . In an equilibrium state, the temperature inside the particle varies linearly along the cylinder axis, and thus its values at the front and back surfaces are written

$$T_f = T_d(1 + \Delta), \quad T_b = T_d(1 - \Delta), \quad (\text{A1})$$

respectively. The energy balance reads

$$I - \epsilon\sigma_{\text{SB}}T_f^4 - q_f = Q_{\text{con}} = \epsilon\sigma_{\text{SB}}T_b^4 + q_b. \quad (\text{A2})$$

We calculate each term of equation (A2). First we consider free molecular photophoresis ($\text{Kn} \gg 1$). The radiative fluxes from the front and back surfaces are, assuming $\Delta \ll 1$,

$$\epsilon\sigma_{\text{SB}}T_f^4 = \epsilon\sigma_{\text{SB}}T_d^4(1 + 4\Delta), \quad \epsilon\sigma_{\text{SB}}T_b^4 = \epsilon\sigma_{\text{SB}}T_d^4(1 - 4\Delta), \quad (\text{A3})$$

respectively. The thermal conduction to the gas at the front surface is divided as

$$q_f = q_f^- - q_f^+, \quad (\text{A4})$$

where q_f^- is the energy loss from the particle that is taken by the gas molecules ejected from the front surface and q_f^+ is the energy gain that is given by the adsorbed molecules. In the free molecular approximation ($\text{Kn} \gg 1$), the velocity distribution of the adsorbed molecules is written $\alpha f^+(\mathbf{v})$, where $0 \leq \alpha \leq 1$ is the accommodation coefficient, $f^+(\mathbf{v})$ is a Maxwellian velocity distribution of temperature T_g and number density n_g ,

$$f^+(\mathbf{v}) = n_g \left(\frac{m_g}{2\pi k_B T_g} \right)^{3/2} \exp \left(- \frac{m_g |\mathbf{v}|^2}{2k_B T_g} \right), \quad (\text{A5})$$

and m_g is the mass of a molecule. We define $f^+(\mathbf{v})$ to be nonzero even for particles going away from the surface ($v_z > 0$). The energy gain is

$$q_f^+ = \alpha \int_{v_z < 0} \frac{m_g v_z}{2} |\mathbf{v}|^2 f^+ d\mathbf{v} = \frac{\alpha P v_T}{2}, \quad (\text{A6})$$

where v_z is the velocity component normal to the front surface, $P = \pi \rho_g v_T^2 / 8$ is the gas pressure, and $v_T = (8k_B T_g / \pi m_g)^{1/2}$ is the mean thermal speed of gas molecules. The molecules ejected from the front surface are assumed to have a Maxwellian velocity distribution, $\alpha f^-(\mathbf{v})$, of temperature T_f . The energy loss is

$$q_f^- = \alpha \int_{v_z > 0} \frac{m_g v_z}{2} |\mathbf{v}|^2 f^- d\mathbf{v} = \frac{\pi}{16} \alpha \rho_f^- (v_f^-)^3, \quad (\text{A7})$$

where $v_f^- = (8k_B T_f / \pi m_g)^{1/2}$ and the “density” of ejected molecules (for $\alpha = 1$) is

$$\rho_f^- = \int_{\text{all } \mathbf{v}} m_g f^- d\mathbf{v}. \quad (\text{A8})$$

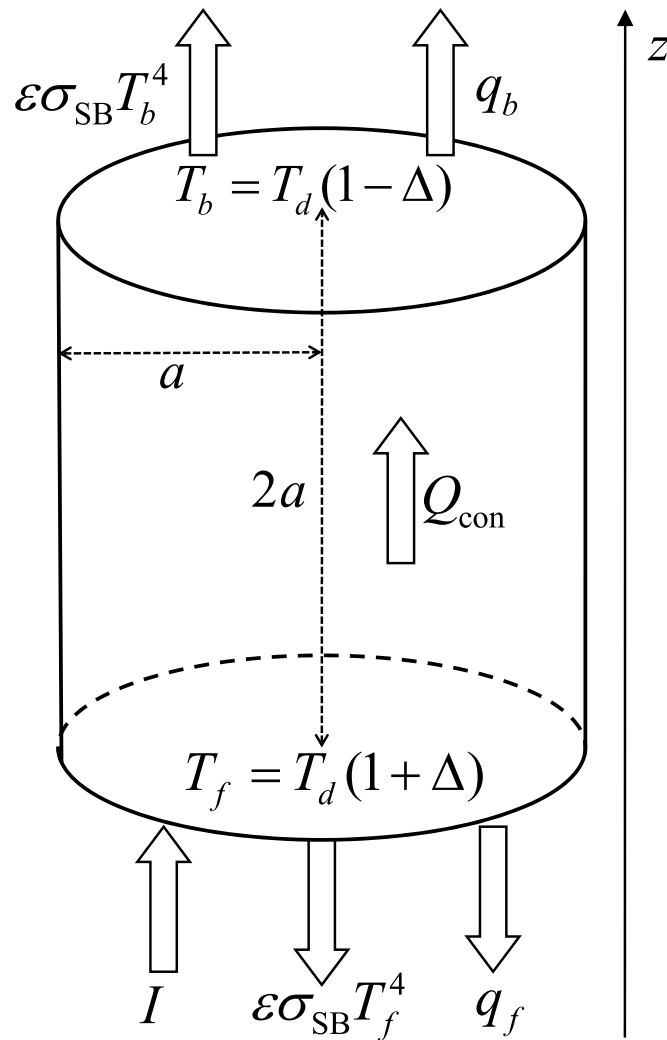


FIG. 9.—A cylindrical dust particle of radius a and height $2a$. The incident stellar flux I is parallel to the cylinder axis (z -axis) and irradiates the front surface. Radiation fluxes from the front and back surfaces are $\epsilon\sigma_{\text{SB}}T_f^4$ and $\epsilon\sigma_{\text{SB}}T_b^4$, respectively. The fluxes of heat conduction to the gas are q_f and q_b , and the heat flux inside the particle is Q_{con} .

From mass conservation between the adsorbed and ejected molecules ($\alpha\rho_f^-v_f^- = \alpha\rho_g v_T$),

$$\rho_f^- = (T_g/T_f)^{1/2}\rho_g. \quad (\text{A9})$$

Then we obtain

$$q_f^- = \frac{1}{2}\alpha P v_T T_f/T_g. \quad (\text{A10})$$

If the gas temperature and the average dust temperature are same ($T_g = T_d$), the thermal conduction to the gas is

$$q_f = \frac{1}{2}\alpha P v_T \Delta. \quad (\text{A11})$$

Similarly, the thermal conduction to the gas from the back surface is

$$q_b = -\frac{1}{2}\alpha P v_T \Delta. \quad (\text{A12})$$

The thermal conduction inside the particle is

$$Q_{\text{con}} = k_d \frac{T_d \Delta}{a}. \quad (\text{A13})$$

Collecting all the above expressions for the terms in equation (A2), the particle temperature is solved as

$$T_d = \left(\frac{I}{2\epsilon\sigma_{\text{SB}}} \right)^{1/4}, \quad (\text{A14})$$

and

$$\Delta = \frac{I}{2(k_d T_d/a + 4\epsilon\sigma_{\text{SB}} T_d^4 + \alpha P v_T/2)}. \quad (\text{A15})$$

The force exerted on the front surface by the ejected molecules is

$$F_f = \pi a^2 \alpha \int_{v_z > 0} m_g v_z^2 f^- dv = \frac{\pi a^2 \alpha P}{2} \left(\frac{T_f}{T_g} \right)^{1/2}, \quad (\text{A16})$$

and on the back surface

$$F_b = \frac{1}{2} \pi a^2 \alpha P (T_b/T_g)^{1/2}. \quad (\text{A17})$$

Assuming $T_g = T_d$ and $\Delta \ll 1$, the photophoretic force is

$$F_{\text{ph},f} = F_f - F_b = \frac{\pi a^2 \alpha I P}{4(k_d T_d/a + 4\epsilon\sigma_{\text{SB}} T_d^4 + \alpha P v_T/2)}, \quad (\text{A18})$$

which can be compared with equation (3) for the case of a spherical particle.

We consider how the photophoretic force changes from equation (A18) when the dust temperature T_d differs from the gas temperature T_g . For simplicity, we consider cases in which the thermal conduction to the gas can be neglected. With $q_f = q_b = 0$ in equation (A2), the photophoretic force becomes

$$F_{\text{ph},f} = \frac{\pi a^2 \alpha I P}{4(k_d T_d/a + 4\epsilon\sigma_{\text{SB}} T_d^4)} \left(\frac{T_d}{T_g} \right)^{1/2}, \quad (\text{A19})$$

which differs from the $T_d = T_g$ case by a factor of $(T_d/T_g)^{1/2}$. We consider further the cases in which the temperature variation inside the dust particle is large ($\Delta \sim 1$). Such a situation arises if $\epsilon\sigma_{\text{SB}} T_d^4 \gg (k_d T_d/a, \alpha P v_T)$. In this case, $T_f = (I/\epsilon\sigma_{\text{SB}})^{1/4}$ and $T_b = 0$, and thus the photophoretic force is $F_{\text{ph},f} = F_f = \frac{1}{2} \pi a^2 \alpha P (T_f/T_g)^{1/2}$. The photophoretic force calculated from equation (A19), which assumes $\Delta \ll 1$, reduces to $F_{\text{ph},f} = F_f/(4 \times 2^{1/8})$ when the term $k_d T_d/a$ is neglected. Thus, in the extreme case where $\Delta \sim 1$, equation (A21) underestimates the photophoretic force by a factor of $4 \times 2^{1/8}$.

In the slip-flow regime ($\text{Kn} \ll 1$), thermal conduction to the gas is estimated as $q_f \sim q_b \sim k_g T_d \Delta/a$, where k_g is the thermal conductivity of the gas. The temperature difference is

$$\Delta \sim \frac{I}{(k_d + k_g) T_d/a + 4\epsilon\sigma_{\text{SB}} T_d^4}. \quad (\text{A20})$$

Because of the temperature variation along the dust surface, a slip flow of the gas arises. The velocity of the thermal slip is

$$v_s \sim C_s v_T \Delta \text{Kn}, \quad (\text{A21})$$

where $C_s \sim 1$ is the thermal slip coefficient (Lifshitz & Pitaevskii 1981). The particle, which moves in the gas with a velocity v_s , experiences Stokes gas drag,

$$F_{\text{Stokes}} \sim a \eta_{\text{vis}} v_s, \quad (\text{A22})$$

where $\eta_{\text{vis}} = l v_T \rho_g/2 = v_T m_g/(2\sqrt{2}\sigma_{\text{mol}})$ is the molecular viscosity. ($F_{\text{Stokes}} = 6\pi a \eta_{\text{vis}} v_s$ if the particle is spherical.) In the equilibrium state, the photophoretic force balances the Stokes drag force and is estimated as

$$F_{\text{ph},s} \sim \frac{C_s a^2 k_B I}{\sigma_{\text{mol}} k_d} \left(1 + \frac{4a\epsilon\sigma_{\text{SB}} T_d^3}{k_d} + \frac{k_g}{k_d} \right)^{-1} \text{Kn}, \quad (\text{A23})$$

which can be compared with equation (5). In the above derivation, we have neglected the temperature jump at the surface and the velocity slip due to imperfect sticking of the gas to the surface ($C_t = C_m = 0$).

APPENDIX B

SLIP-FLOW REGIME PHOTOPHORESIS

In this appendix, we derive the expression for the photophoretic force in the slip-flow regime (eq. [5]), taking into account the radiative cooling of the particle. We follow the derivation described by Mackowski (1989). (The assumptions are as follows: The mean temperatures of the gas and the dust, T_g and T_d , are the same. The temperature variation from the mean value is small. The Reynolds number is much less than unity and thus gas drag obeys the Stokes law. The gas temperature is determined only by the heat conduction from the dust and inside the gas.) Here we do not rewrite Mackowski's derivation, but we describe what is modified when radiative cooling is taken into account. The numbering of equations with "M" means that they refer to equations of Mackowski (1989). For the meaning of the symbols see Mackowski (1989). However, for some variables we have used different symbols in the main text, and we keep the same notation here. When we use a symbol different from Mackowski's, the corresponding symbol from Mackowski (1989) is given in parentheses.

The basic equations (M11)–(M14) and the boundary conditions (M15)–(M20) are not changed, except that equation (M16) is modified as

$$-k_g \frac{\partial \hat{T}_g}{\partial r} + \epsilon \sigma_{\text{SB}} \hat{T}_d^4 = -k_d \frac{\partial \hat{T}_d}{\partial r}, \quad (\text{B1})$$

where $\hat{T}_d(T_s)$ is the temperature inside the dust particle, $\hat{T}_g(T_g)$ is the gas temperature, and $k_d(k_s)$ is the thermal conductivity of the dust. Then equation (M22) becomes

$$D_n = \frac{nG_n(1) - G'_n(1)}{(4\epsilon\sigma_{\text{SB}}T_d^3 a/k_d + n)[1 + (n+1)C_{tl}/a] + (n+1)k_g/k_d}, \quad (\text{B2})$$

where $T_d(T_0)$ is the mean temperature of the dust, $C_t(c_t)$ is the coefficient of the jump condition, and we have corrected a typo in the sign of the original equation. Equation (M28) is not modified when it is expressed using D_1 as

$$c_1 = \frac{3(1 + 2C_{ml}/a)}{4(1 + 3C_{ml}/a)} - \frac{C_s \eta_{\text{vis}} D_1}{2V_0 \rho_g a (1 + 3C_{ml}/a)}, \quad (\text{B3})$$

where $\eta_{\text{vis}}(\eta)$ is the molecular viscosity and $C_m(c_m)$ and $C_s(c_s)$ are the coefficients of the jump conditions. Finally, equation (M29) becomes

$$F_p = -\frac{4\pi C_s \eta_{\text{vis}}^2 a I J_1}{k_d T_d \rho_g} \frac{1}{(1 + 3C_{ml}/a)[(4\epsilon\sigma_{\text{SB}}T_d^3 a/k_d + 1)(1 + 2C_{tl}/a) + 2k_g/k_d]}, \quad (\text{B4})$$

where $I(I_\lambda)$ is the incident flux of the starlight. Substitution of the expression for $\eta_{\text{vis}}^2 = \sqrt{2} l \rho_g k_B T_d / (\pi \sigma_{\text{mol}})$ and taking the absolute value gives equation (5).

REFERENCES

- Alexander, D. R., & Ferguson, J. W. 1994, *ApJ*, 437, 879
 Alexander, R. D., Clarke, C. J., & Pringle, J. E. 2006a, *MNRAS*, 369, 216
 ———. 2006b, *MNRAS*, 369, 229
 Ardila, D. R., et al. 2005, *ApJ*, 627, 986
 Augereau, J.-C., Lagrange, A. M., Mouillet, D., & Ménard, F. 1999, *A&A*, 350, L51
 Beresnev, S., Chernyak, V., & Fomyagin, G. 1993, *Phys. Fluids A*, 5, 2043
 Borysow, A., Jørgensen, U. G., & Zheng, C. 1997, *A&A*, 324, 185
 Bottke, W. F., Jr., Vokrouhlický, D., Rubincam, D. P., & Broz, M. 2002, in *Asteroids III*, ed. W. F. Bottke, Jr., et al. (Tucson: Univ. Arizona Press), 395
 Brownlee, D., et al. 2006, *Science*, 314, 1711
 Burns, J. A., Lamy, P. L., & Soter, S. 1979, *Icarus*, 40, 1
 Chapman, S., & Cowling, T. G. 1970, *The Mathematical Theory of Non-Uniform Gases* (3rd ed.; Cambridge: Cambridge Univ. Press)
 Chen, C. H., & Kamp, I. 2004, *ApJ*, 602, 985
 Clampin, M., et al. 2003, *AJ*, 126, 385
 Clarke, C. J., Gendrin, A., & Sotomayor, M. 2001, *MNRAS*, 328, 485
 Coulson, I. M., Dent, W. R. F., & Greaves, J. S. 2004, *MNRAS*, 348, L39
 Cuzzi, J. N., Hogan, R. C., Paque, J. M., & Dobrovolskis, A. R. 2001, *ApJ*, 546, 496
 Dent, W. R. F., Greaves, J. S., & Coulson, I. M. 2005, *MNRAS*, 359, 663
 Dullemond, C. P., & Dominik, C. 2005, *A&A*, 434, 971
 Ferguson, J. W., Alexander, D. R., Allard, F., Barman, T., Bodnarik, J. G., Hauschildt, P. H., Heffner-Wong, A., & Tamanai, A. 2005, *ApJ*, 623, 585
 Fisher, R. S., Telesco, C. M., Piña, R. K., Knacke, R. F., & Wyatt, M. C. 2000, *ApJ*, 532, L141
 Goto, M., Usuda, T., Dullemond, C. P., Henning, T., Linz, H., Stecklum, B., & Suto, H. 2006, *ApJ*, 652, 758
 Greaves, J. S. 2004, *MNRAS*, 351, L99
 Greaves, J. S., Mannings, V., & Holland, W. S. 2000, *Icarus*, 143, 155
 Hartmann, L., Calvet, N., Gullbring, E., & D'Alessio, P. 1998, *ApJ*, 495, 385
 Hayashi, C., Nakazawa, K., & Nakagawa, Y. 1985, in *Protostars and Planets II*, ed. D. C. Black & M. S. Matthews (Tucson: Univ. Arizona Press), 1100
 Hidy, G. M., & Brock, J. R. 1967, *J. Geophys. Res.*, 72, 455
 Hollenbach, D., Johnstone, D., Lizano, S., & Shu, F. 1994, *ApJ*, 428, 654
 Krauss, O., & Wurm, G. 2005, *ApJ*, 630, 1088
 Krauss, O., Wurm, G., Mousis, O., Petit, J.-M., Horner, J., & Alibert, Y. 2007, *A&A*, 462, 977
 Krivov, A. V., Löhne, T., & Sremčević, M. 2006, *A&A*, 455, 509
 Lifshitz, E. M., & Pitaevskii, L. P. 1981, *Physical Kinetics* (Oxford: Pergamon)
 Liseau, R., & Artymowicz, P. 1998, *A&A*, 334, 935
 Mackowski, D. W. 1989, *Int. J. Heat Mass Transfer*, 32, 843
 Marsh, K. A., Silverstone, M. D., Becklin, E. E., Koerner, D. W., Werner, M. W., Weinberger, A. J., & Ressler, M. E. 2002, *ApJ*, 573, 425
 Miyake, K., & Nakagawa, Y. 1993, *Icarus*, 106, 20
 Mouillet, D., Lagrange, A. M., Augereau, J.-C., & Ménard, F. 2001, *A&A*, 372, L61
 Mousis, O., Petit, J.-M., Wurm, G., Krauss, O., Alibert, Y., & Horner, J. 2007, *A&A*, 466, L9
 Nakagawa, Y., Sekiya, M., & Hayashi, C. 1986, *Icarus*, 67, 375
 Nomura, H., & Nakagawa, Y. 2006, *ApJ*, 640, 1099
 Petit, J.-M., Mousis, O., Alibert, Y., & Horner, J. 2006, in *Lunar and Planetary Science XXXVII* (Houston: Lunar Planet. Inst.), No. 1558
 Presley, M. A., & Christensen, P. R. 1997, *J. Geophys. Res.*, 102, 6535
 Strubbe, L. E., & Chiang, E. I. 2006, *ApJ*, 648, 652
 Takeuchi, T., & Artymowicz, P. 2001, *ApJ*, 557, 990

- Takeuchi, T., Clarke, C. J., & Lin, D. N. C. 2005, *ApJ*, 627, 286
Tanaka, H., Himeno, Y., & Ida, S. 2005, *ApJ*, 625, 414
Thébault, P., & Augereau, J.-C. 2005, *A&A*, 437, 141
Tsuji, T. 1966, *PASJ*, 18, 127
———. 1971, *PASJ*, 23, 553
———. 2002, *ApJ*, 575, 264
Weidenschilling, S. J. 1984, *Icarus*, 60, 553
Weidenschilling, S. J., & Cuzzi, J. N. 1993, in *Protostars and Planets III*, ed. E. H. Levy & J. I. Lunine (Tucson: Univ. Arizona Press), 1031
Weinberger, A. J., Becklin, E. E., Schneider, G., Smith, B. A., Lowrance, P. J., Silverstone, M. D., Zuckerman, B., & Terile, R. J. 1999, *ApJ*, 525, L53
Weinberger, A. J., Rich, R. M., Becklin, E. E., Zuckerman, B., & Matthews, K. 2000, *ApJ*, 544, 937
Wurm, G., & Krauss, O. 2006, *Icarus*, 180, 487
Wyatt, M. C. 2006, *ApJ*, 639, 1153
Zuckerman, B., Forveille, T., & Kastner, J. H. 1995, *Nature*, 373, 494